http://dx.doi.org/10.1097/mm9.0000000000000003

MedMat

Review

OPEN

Mechanism and design of organic afterglow luminescent probes for cancer theranostics

Zhiyuan Gao[a], Yifei Zhang[b], Qian Liu[b], Dan Ding[a,*]

Abstract

Organic afterglow luminescent probes (OALPs), characterized by their long-lasting luminescence after irradiation (by light, ultrasound, or X-rays) cessation, are pivotal tools in autofluorescence-free optical imaging. They exhibit ultra-low background noise interference, enhancing imaging sensitivity and ensuring clearer, more reliable imaging results. Moreover, they offer deeper tissue penetration compared to traditional optical imaging modalities, providing various information from deep tissues. Recently developed sonoafterglow and radioafterglow further enhance tissue penetration depth. This review outlines 2 design approaches for OALPs: coencapsulation and conjugation, which are derived from their luminescent mechanism. Guided by these strategies, researchers have designed 3 types of OALPs: near-infrared OALPs, responsive OALPs, and ratiometric OALPs. Additionally, we also provided examples of how OALPs are integrated with therapy and applied in the field of cancer theranostics. Finally, we discuss certain challenges encountered in the advancement of the next generation of OALPs, aiming to broaden their scope of applications.

Keywords: Afterglow imaging, Cancer theranostics, Design strategy, Luminescent mechanism, Organic afterglow luminescent probes

1. Introduction

Optical imaging technology presents prominent advantages in both biological and medical fields.[1,2] Compared to tomographic imaging techniques such as magnetic resonance imaging, computed tomography (CT), and positron emission tomography, optical imaging boasts high spatiotemporal resolution, enabling real-time investigation of molecular and biological processes.[3,4] Its cost-effectiveness facilitates widespread adoption in clinical and research settings, while its noninvasive nature and real-time imaging capabilities render it a safe and efficient medical tool.[5] However, most optical imaging techniques rely on real-time fluorescence signals generated by light excitation, where background noise from endogenous molecules within biological specimens is unavoidable.[6] This leads to the minimization of signal-to-background ratio (SBR) and limited penetration depth, thereby affecting imaging sensitivity and ultimately reducing the reliability of the signal and image quality.[7] The emergence of bioluminescent and chemiluminescent self-luminescent probes has indeed partially addressed the background noise issue in optical imaging technology.[8] However, bioluminescent imaging and chemiluminescent imaging rely on enzyme-catalyzed or chemical reactions to trigger the luminescence of specific materials.[9,10] While bioluminescent and chemiluminescent probes do not need real-time excitation, they still require activation through interactions with specific endogenous enzymes or chemical stimuli.[11,12] Therefore, their application in vivo is inevitably restricted. Afterglow imaging probes possess the characteristic of emitting long-lasting light after irradiation (by light, ultrasound, or X-rays) ceases.[13] Afterglow imaging relies on external irradiation, with the irradiation and signal acquisition processes separated.[14] This segregation effectively eliminates background and autofluorescence interference, significantly enhancing SBR and the sensitivity of imaging.[15,16]

Afterglow imaging probes can be categorized into 2 types: inorganic afterglow imaging probes and organic afterglow luminescent probes (OALPs). Inorganic afterglow imaging probes are typically based on doping rare-earth elements or other transition metal ions.[17,18] However, due to the potential risk of leakage of toxic heavy metal ions, the use of inorganic materials in biomedical applications may be impacted.[19,20] In contrast, OALPs are safer and offer advantages such as flexible synthesis and lower production costs.[21] They can be easily modified with targeting groups to enhance their targeting capability toward specific lesion sites.[22] OALPs used for theranostics need to possess both diagnostic and therapeutic effects simultaneously. The combined diagnostic and therapeutic functionality allows for early disease detection and immediate initiation of therapy, reducing the delay between diagnosis and therapy.[23] Additionally, it can provide real-time information to assist physicians in adjusting therapeutic parameters, facilitating personalized therapy and avoiding ineffective or excessive therapy.[24]

In this review, we primarily summarize the mechanism and design strategies of existing OALPs. Subsequently, we introduce their applications in surgical therapy, photodynamic therapy, photothermal therapy, radiodynamic therapy, chemotherapy, and immunotherapy. Finally, we share our suggestions and

[a]Frontiers Science Center for Cell Responses, State Key Laboratory of Medicinal Chemical Biology, Key Laboratory of Bioactive Materials, Ministry of Education, and College of Life Sciences, Nankai University, Tianjin, China, [b]Department of Urology, Tianjin First Central Hospital, Tianjin, China.

**Corresponding author: Address: Dan Ding, College of Life Sciences, Nankai University, Tianjin 300071, China. E-mail address: dingd@nankai.edu.cn (D. Ding).*

MedMat (2024) 1:1

Received: 29 February 2024; Accepted 2 June 2024

Published online 13 August 2024

opinions regarding the current issues and challenges of organic afterglow imaging in biomedical applications. To the best of our knowledge, there is currently no review of the design strategies of OALPs. Therefore, it is essential to provide a detailed summary to assist researchers interested in designing OALPs.

2. Luminescent mechanism

Currently, the luminescence mechanism of OALPs used in in vivo imaging can be summarized as follows. Under the mediation of singlet oxygen ($^1O_2$), radiation energy is stored in the afterglow substrate, forming the high-energy and unstable 1,2-dioxetane structure. Subsequently, the 1,2-dioxetane gradually decomposes and transfers the energy released from the bond cleavage within or between molecules. Finally, the energy receptor with fluorescence properties releases the energy in the form of photons, known as "afterglow." According to the luminescence mechanism of OALPs, 3 components are required: (1) afterglow initiator, responsible for absorbing and converting irradiation energy into $^1O_2$; (2) afterglow substrate, responsible for reacting with $^1O_2$ to form the high-energy and unstable afterglow intermediate (1,2-dioxetane); (3) fluorophore acts as the afterglow relay unit, responsible for accepting energy from 1,2-dioxetane and gradually releasing it in the form of photons (Fig. 1). Based on these 3 components summarized for OALPs, we can use them to guide the design of OALPs.

3. Design strategy

3.1 Coencapsulation

The coencapsulation strategy involves encapsulating 2 or more molecules together using self-assembly of amphiphilic compounds. This strategy offers high flexibility, allowing for easy adjustment of the proportions between molecules to achieve synergistic effects. Applying this strategy to the development of OALPs enables the easy concentration of the 3 components: afterglow initiator, afterglow substrate, and afterglow relay unit through π–π interactions, facilitating chemical reactions and energy transfer processes between them.

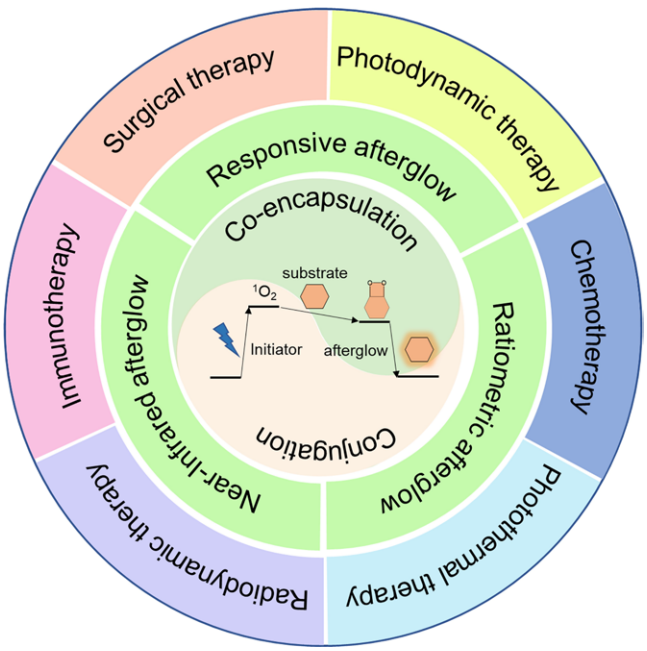

Figure 1. Scheme illustrating the design strategy and luminescent mechanism of OALPs for cancer theranostics.

3.1.1 Near-Infrared OALPs

Near-infrared (NIR) imaging is a noninvasive imaging technique known for its strong tissue penetration and high imaging resolution.[25,26] Combining afterglow imaging with NIR imaging can further enhance imaging effectiveness, enabling more accurate and sensitive detection of biological tissues. However, the variety of OALPs and their afterglow spectra is quite limited, which hampers their widespread application in biomedical imaging. To address this issue, Jiang et al proposed an innovative strategy for converting common fluorophores into afterglow luminescent nanoparticles (Fig. 2A).[27] The advent of this universal strategy allows for the utilization of nearly all existing fluorophores to obtain afterglow probes of different wavelengths, greatly enriching the material resources for afterglow imaging. This strategy involves coencapsulating the afterglow initiator, afterglow substrate, and afterglow relay unit within the same nanoparticle, achieving precise control over the luminescence of afterglow probes. By adjusting the doping ratio of each component within the nanoparticles, the emission wavelength of afterglow can be finely tuned, covering the entire spectrum from visible light to the NIR region. Additionally, Ni et al coencapsulated aggregation-induced emission (AIE) luminogens and afterglow substrate within the same nanoparticle, leading to the development of NIR-emitting afterglow AIE dots (Fig. 2B).[28] Leveraging the high fluorescence quantum yield and singlet oxygen generation efficiency of AIE luminogens in confined spaces (inside nanoparticles), the luminescence brightness and afterglow time of NIR-emitting afterglow AIE dots are significantly higher than those of pure afterglow substrate yellow-green emitting dots. This further confirms the importance of the AIE effect in enhancing afterglow imaging.

3.1.2 Responsive OALPs

The previously mentioned OALPs do not rely on biomarkers and their afterglow luminescence often remains in an undistinguished "always on" state, which heavily relies on the concentration difference between the lesion site and normal tissues during disease imaging, leading to poor specificity.[29,30] Responsive OALPs refer to afterglow luminescence regulated by biomarkers, aiming to further enhance signal specificity and diagnostic accuracy. Wu et al reported an OALP responsive to the biomarker hydrogen sulfide (H_2S), which exhibits specific afterglow luminescence only under the influence of H_2S (Fig. 3A).[31] First, the authors carefully designed $F1^{2+}$ as a chromophore responsive to H_2S, ensuring that its spectrum extensively overlaps with that of afterglow nanoparticle (ANP) composed of the afterglow substrate MEH-PPV and the afterglow initiator NIR775 in the "always on" state. After incorporating $F1^{2+}$ into the nanoparticles, the fluorescence and singlet oxygen generation abilities of MEH-PPV and NIR775 are both quenched by $F1^{2+}$, attributed to the effective fluorescence resonance energy transfer (FRET) from MEH-PPV and NIR775 to $F1^{2+}$. In the presence of H_2S, $F1^{2+}$ rapidly reverts to F2 with a significantly blue-shifted absorption, eliminating the FRET process and allowing F2-ANP to regain singlet oxygen production and fluorescence under light irradiation, thereby activating the afterglow luminescence. Additionally,

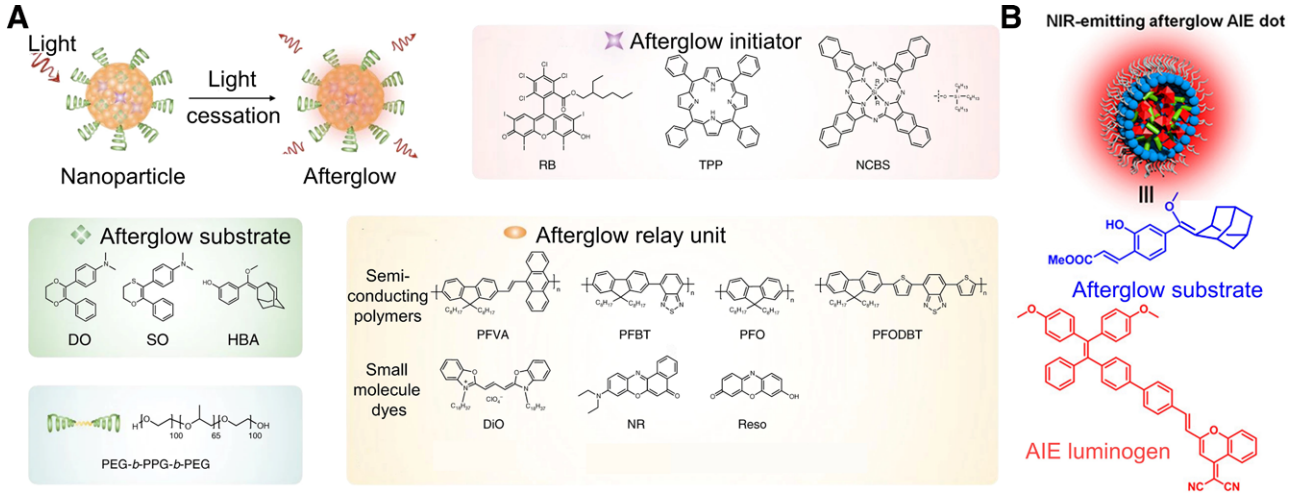

Figure 2. Design strategy of coencapsulation of near-infrared OALPs. (A) Scheme illustrating the composition of afterglow luminescence nanoparticle (ALNP) and its chemical structure. Adapted with permission from Jiang et al.[27] (B) The chemical structural formulas of afterglow substrate and AIE luminogens. Adapted with permission from Ni et al.[28]

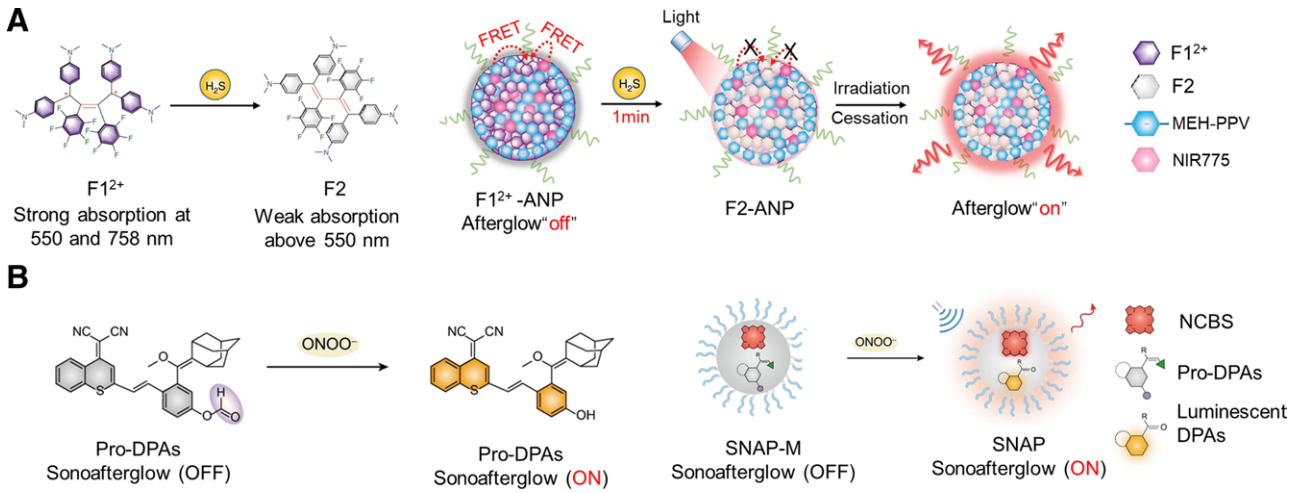

Figure 3. Design strategy of coencapsulation of responsive OALPs. (A) The chemical structures of the $F1^{2+}$ before and after reacting to H_2S to form F2, accompanied by a scheme illustrating the composition of $F1^{2+}$-ANP in the off state and F2-ANP in the on state. Adapted with permission from Wu et al.[31] (B) The chemical structures of the Pro-DPAs before and after reacting to $ONOO^-$ to form DPAs, accompanied by a scheme illustrating the composition of SNAP-M in the off state and SNAP in the on state. Adapted with permission from Xu et al.[32]

Xu et al developed an activatable sonoafterglow nanoparticle (SNAP-M), which only activates its sonoafterglow luminescence in the presence of the specific disease biomarker (Fig. 3B).[32] The authors first prepared sonoafterglow nanoparticles, comprising a sonosensitizer NCBS, which acts as an afterglow initiator to generate $^1O_2$ and an afterglow substrate Pro-DPAs with a peroxynitrite ($ONOO^-$)-responsive cage moiety. In the presence of $ONOO^-$, the responsive moiety on Pro-DPAs is decaged, activating the afterglow luminescence capability as the afterglow substrate. Due to the greater penetration of energy generated by ultrasound, it exhibits a brighter and deeper emission compared to previously reported light-induced afterglow luminescence, even reaching tissue depths of up to 4 cm. The innovation brought by sonoafterglow imaging technology not only lies in the brightness and depth of the signal but also provides a potential solution for a wider range of biomedical applications. Building upon the previous research on NIR-emitting afterglow AIE dots, Chen et al further designed and synthesized a dual-responsive OALPs sensitive to both $ONOO^-$ and pH.[33] In the presence of $ONOO^-$ at physiological pH, it exhibits activated near-infrared afterglow luminescence, with its intensity and lasting time significantly enhanced by introducing the AIE effect.

3.1.3 Ratiometric OALPs

Although responsive OALPs can be selectively activated for specific biomarkers and quantitatively analyzed, the increasing decay of afterglow intensity over time adds complexity to quantitative analysis.[2] Additionally, the intensity of afterglow is influenced by factors such as laser power, irradiation time, and exposure time, further complicating the system.[34] Liu et al has reported a ratiometric afterglow nanoplatform (RAN) that can be used to tailor various responsive OALPs and precisely quantify specific biomarker analytes (Fig. 4).[35] The authors encapsulated responsive molecules (NRM, ORM, or PRM), afterglow substrates, and afterglow initiators within the same nanoparticle. Following light irradiation, the afterglow initiator generates singlet oxygen, prompting the release of shorter-wavelength afterglow luminescence (AF2) from the afterglow substrate, which is then gradually transferred to

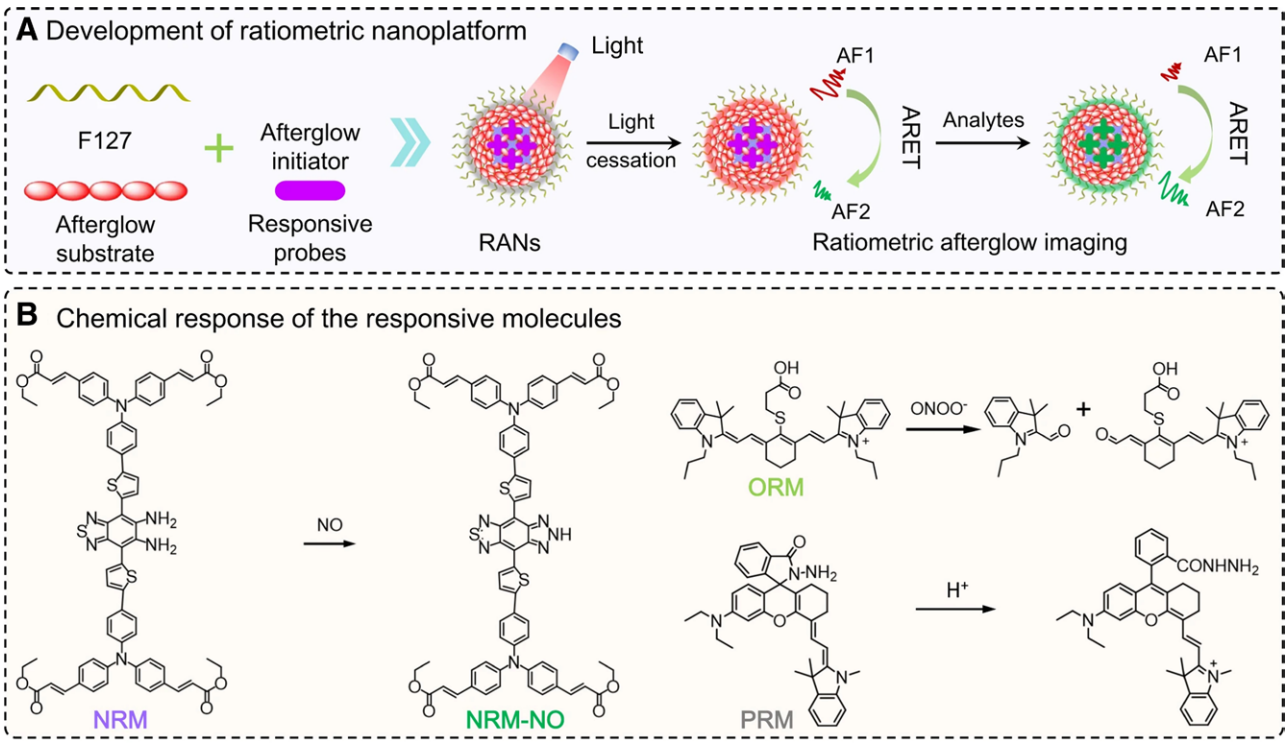

Figure 4. Scheme illustrating the composition of RANs and ARET-based ratiometric afterglow before and after analytes respond (A). The chemical structures of the responsive molecules before and after response to NO, $ONOO^-$, and pH (B). Adapted with permission from Liu et al.[35]

responsive molecules emitting longer-wavelength afterglow luminescence (AF1) via afterglow resonance energy transfer (ARET). Consequently, quantitative detection of biomarkers can be achieved by calculating the ratio of afterglow intensity (AF1/AF2) between the afterglow energy donor (afterglow substrate) and energy acceptor (responsive molecules). The ratios of afterglow intensities would be independent of interference factors other than analytes, which not only address the decay of afterglow intensity but also eliminate interference from various factors (such as laser power, irradiation time, and exposure time), thereby facilitating reliable quantitative analysis in biological systems.

3.2 Conjugation

In addition to the coencapsulation strategy, there is also an integrated conjugation strategy. Unlike the coencapsulation strategy that requires intermolecular resonance energy transfer, the conjugation strategy concentrates all functional units (including units for $^1O_2$ generation units, $^1O_2$ capturing units, and luminescent units) within a single molecule, utilizing intramolecular energy transfer for luminescence. Thus, this strategy of molecular OALPs eliminates the need for spectral overlap in coencapsulation and enhances system reliability.

3.2.1 Near-Infrared OALPs

The design strategies for near-infrared luminescent moieties primarily fall into 2 categories: (1) extending conjugated structures and (2) modulating the push-pull electronic capabilities of donor and acceptor groups. Therefore, conjugation can be utilized to extend afterglow substrates into the near-infrared region. However, not all afterglow substrates extended into the near-infrared region possess the capability to emit afterglow luminescence and also need to have the ability to generate $^1O_2$. Yang et al utilized the characteristics of porphyrin derivatives, which possess both near-infrared emission wavelengths and excellent $^1O_2$ generation capabilities (Fig. 5A).[36] They chemically conjugated the afterglow substrate (DO) with the NIR photosensitizer tetraphenylporphyrin (TPP), forming TPP-DO. When light irradiation, TPP-DO generates $^1O_2$, oxidizing itself to an unstable TPP-DO-dioxetane intermediate. This intermediate spontaneously decomposes into the ester derivative TPP-DE, while simultaneously absorbing the energy released during the decomposition process to form the excited state TPP-DE*. TPP-DE* ultimately releases the absorbed energy in the form of NIR light as it returns to the ground state TPP-DE. This intramolecular energy transfer from the afterglow substrate to the energy release unit significantly enhances the afterglow brightness compared to intermolecular energy transfer. Semiconductor polymers comprise an extended π-conjugated structure. Recently, it has been discovered that poly(*p*-phenylenevinylene) (PPV)-based semiconductor polymers are also excellent afterglow substrates.[37] However, they can only emit visible light and have moderate $^1O_2$ generation capability. Cui et al copolymerized the NIR photosensitizer TPP into the PPV to obtain PPV-TPP.[38] In comparison to PPV, PPV-TPP not only exhibits NIR afterglow luminescence but also possesses amplified afterglow intensity. Liao et al reported a novel NIR semiconductor polymer (named NIR-3) containing a donor–acceptor conjugated structure capable of producing intense afterglow luminescence in the NIR window (Fig. 5B).[39] NIR-3's backbone structure contains abundant thiophene as the donor and introduces pyrido pyrazine as the acceptor. This donor–acceptor structure not only shifts the emission wavelength to the red but also enhances the intersystem crossing

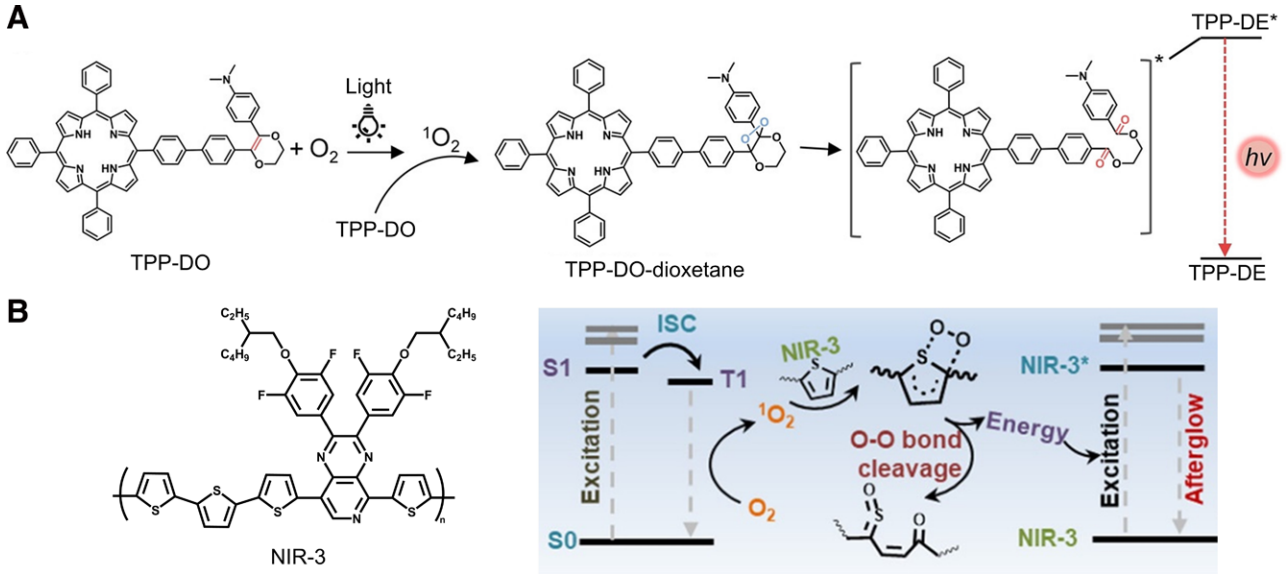

Figure 5. Design strategy of conjugation of near-infrared OALPs. (A) The chemical structures of TPP-DO and proposed mechanism for the afterglow luminescence of TPP-DO. Adapted with permission from Yang et al.[36] (B) The chemical structures of NIR-3 and proposed mechanism for the afterglow luminescence of NIR-3. Adapted with permission from Liao et al.[39]

process, thus increasing the production of $^1O_2$. Additionally, a large number of $^1O_2$-reactive thiophene groups can effectively form unstable high-energy thiophene-dioxetane intermediates, followed by peroxide (O–O) bond cleavage to release energy, which is absorbed by NIR-3 itself to form excited state NIR-3* for afterglow luminescence. The integrated conjugation strategy eliminates the need for complex component modulation, allowing a single molecule to fulfill all the requirements for afterglow luminescence.

3.2.2 Responsive OALPs

The design strategies for responsive molecular OALPs primarily fall into 2 categories: (1) destruction and restoration of conjugated skeletons; (2) enhancement and inhibition of intramolecular charge transfer (ICT). Lei et al integrated responsive units, $^1O_2$ generation units, $^1O_2$ capturing units, and luminescent units into a single molecule (Fig. 6A).[40] When responsive units encounter H^+, the probe undergoes a conformational change from a spirocyclic to an open structure, transitioning the molecular structure from nonconjugated to conjugated, ultimately leading to the activation of $^1O_2$ and fluorescence. When light irradiates the open structure, the generated $^1O_2$ oxidizes the $^1O_2$ capturing unit to form unstable high-energy dioxetane intermediates. These intermediates gradually decompose and release excitation energy to the decomposed molecules themselves, resulting in afterglow luminescence. Additionally, the researchers have expanded the application scope of this afterglow molecular scaffold by introducing various biomarkers (ATP or metal ions) responsive units. The same research group also designed hemicyanine-based molecular scaffolds with responsive afterglow luminescence.[41] They similarly employed the "four-in-one" molecular design strategy, integrating responsive units, $^1O_2$ generation units, $^1O_2$ capturing units, and luminescent units into a single molecule, customizing it for the quantification and imaging of targets such as pH, superoxide anions, and aminopeptidase. The responsive units can modulate the activation of fluorescence and the generation of $^1O_2$ by altering the ICT of the entire molecule, thus enabling activatable afterglow luminescence. The issue of tissue penetration depth during excitation can be addressed by ultrasound and similarly, X-rays can also overcome tissue penetration challenges.[42] However, organic molecules often contain light atoms (such as hydrogen, carbon, and oxygen) and exhibit weak spin-orbit coupling, resulting in weak X-ray absorption. Huang et al integrated responsive units, $^1O_2$ generation units, $^1O_2$ capturing units, and luminescent units into a single molecule, to prepare a molecular radioafterglow dynamic probe (MRAP) for radioafterglow luminescence (Fig. 6B).[43] They replaced hydrogen atoms in the benzene ring with heavy iodine atoms to form a new conjugated structure. The introduction of iodine atoms not only enhances the probe's X-ray absorption but also allows a large number of electrons to exist as triplet excitons (Tn). In the absence of cathepsin B (CatB) response, the reduced electron-donating ability of the oxygen atom in the phenolic moiety inhibits the ICT, resulting in negligible radioafterglow luminescence and radiodynamic $^1O_2$ generation. Upon encountering CatB, the responsive moiety is cleaved to liberate uncaged MRAP ($IDPA_{SU}$), restoring fluorescence and radiodynamic $^1O_2$ generation. The specific process involves X-ray photons first exciting high-energy electrons, which then interact with surrounding atoms, initiating a secondary electron cascade with decreased energy. Upon absorption by $IDPA_{SU}$, a large number of electrons exist as triplet excitons, transitioning back to the ground state and exciting triplet oxygen ($^3O_2$) to $^1O_2$. The in situ generated $^1O_2$ reacts with IDPAs to form dioxetane intermediates. Eventually, these intermediates gradually decompose into the corresponding activated products (activated IDPAx), emitting radioafterglow luminescence.

The afterglow imaging offers higher SBR and sensitivity in vivo compared to fluorescence imaging. However, it requires several seconds to minutes for data acquisition, whereas fluorescence imaging only takes a few hundred microseconds. To overcome this limitation, further enhancement of the brightness of OALPs is necessary. Currently, the screening of high-brightness OALPs designed using a coencapsulation strategy still primarily relies on the random combination of different components, which is relatively complex. To address

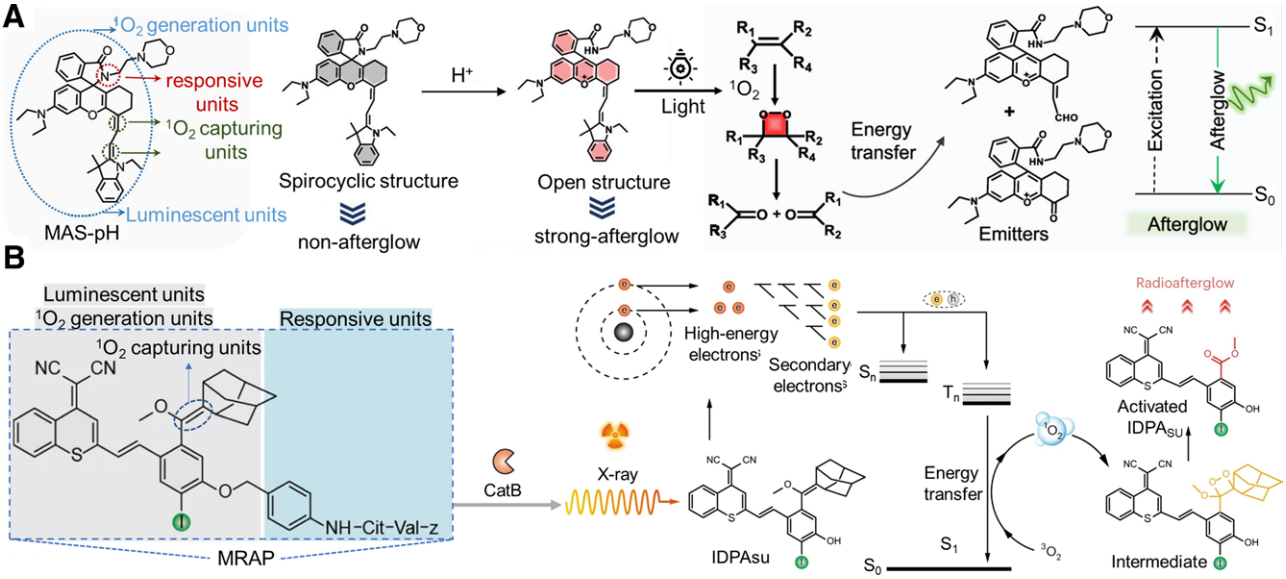

Figure 6. Design strategy of conjugation of responsive OALPs. (A) The chemical structures of MAS-pH before and after responding to H^+, accompanied by the proposed mechanism for the afterglow luminescence of the responsive molecules. Adapted with permission from Lei et al.[40] (B) The chemical structures of MRAP before and after responding to CatB to form IDPAsu, accompanied by the proposed mechanism for the radioafterglow luminescence of IDPAsu. Adapted with permission from Huang et al.[40]

this challenge, we believe it is essential not only to consider the individual energy conversion efficiencies of the afterglow initiator, afterglow substrate, and afterglow relay unit but also the energy transfer efficiencies among these components. For example, to more effectively transfer the $^1O_2$ generated by the afterglow initiator to the afterglow substrate, it is required that the afterglow substrate has a higher rate of producing 1,2-dioxetane intermediate when reacting with $^1O_2$. The high oxidizability of the afterglow substrate is apparently beneficial to this process. Additionally, to enhance the transfer of emitted light energy from the afterglow substrate to the afterglow relay unit, improving the resonance energy transfer efficiency between them is crucial. This might require better spectral overlap between the emission spectrum of the afterglow substrate and the absorption spectrum of the afterglow relay unit. Therefore, optimizing both the individual properties and the interactions among the components is vital for advancing the brightness of OALPs.

For the OALPs designed using the conjugation strategy, although the intramolecular energy transfer from the afterglow substrate to the energy release unit significantly enhances afterglow brightness compared to intermolecular energy transfer, such probes still lack sufficient brightness. To address this challenge, we propose focusing on the relationship between the molecular structure of conjugated probes and their afterglow intensity, continuously improving their brightness.

For near-infrared OALPs, molecular imaging in the second near-infrared (NIR-II, 1000–1700 nm) window has already provided high-resolution imaging with subcentimeter tissue depth. In the future, utilizing OALPs emitting in the NIR-II window could further enhance penetration depth and imaging resolution. However, existing energy donors often emit at shorter wavelengths, requiring multiple energy transfers to successfully shift their emission to the NIR-II region, resulting in significant energy loss. To address this challenge, we propose chemically modifying the energy donors to directly extend their conjugation length, thus extending their emission wavelength to the NIR-II window.

Responsive OALPs enable quantitative analysis of target analytes. However, the presence of various interference factors in afterglow luminescence results in decreased signal reliability. To address this challenge, the design of ratiometric OALPs enables reliable quantification and molecular imaging of specific analytes. This approach mitigates interference from factors such as laser parameters, penetration depth, and probe concentration, significantly enhancing the reliability of afterglow signals.

The primary challenges in the design of ratiometric OALPs is the lack of responsive probes for constructing ratiometric OALPs. This is attributed to the inert nature of most probe structures, lacking reactive sites. Previously reported ratio afterglow probes have been limited to detecting reactive oxygen and nitrogen species or pH levels. However, many physiological and pathological processes involve the excessive production of these biomarkers, rendering precise and specific disease monitoring highly challenging. Therefore, there is still a need for the development of more specific responsive molecular probes, which remains to be explored.

4. Application in cancer theranostics

Cancer, as a malignant tumor, has emerged as a significant cause of human mortality, posing a grave threat to human health.[44] Consequently, considerable importance is placed on researching cancer theranostics, where targeted delivery to tumor sites using probes plays a crucial role.[45] The targeting of tumors can be classified into 2 categories. (1) Active targeting involves the use of specific targeting molecules or carriers to bind with tumor cells, enabling precise diagnosis and therapy.[46] (2) Passive targeting, on the other hand, capitalizes on physiological differences between tumor and normal tissues, such as the enhanced permeability and retention (EPR) effect, to facilitate the accumulation of drugs or diagnostic agents within tumor tissues.[47] The advantages of cancer theranostics lie in assisting in formulating personalized therapy plans, monitoring therapy efficacy, reducing delays and redundant examinations, and achieving personalized cancer therapy.[48,49]

Near-infrared emission wavelength is an ideal wavelength for biological imaging due to its low tissue absorption and scattering, as well as strong tissue penetration. Therefore, it is suitable for cancer theranostics, such as image-guided surgical therapy and monitoring the effects of photodynamic therapy, photothermal therapy, and radiodynamic therapy (Table 1). Responsive OALPs can respond to specific biomolecules or environmental conditions, such as granzyme B, peroxynitrite ($ONOO^-$), and pH value. This responsiveness allows OALPs to provide specific diagnostic information in cancer treatment, help evaluate the effectiveness of chemotherapy and immunotherapy, and track the release of chemotherapy drugs. Ratiometric OALPs, based on responsive OALPs, address the issue of afterglow intensity attenuation over time and eliminate interference from various factors (such as laser power, irradiation time, and exposure time), making them more suitable for reliable quantitative analysis in biological systems.

4.1 Surgical therapy

The use of NIR fluorescence imaging for guiding cancer surgical therapy has emerged as a powerful strategy in clinical practice, aiding surgeons in faster and more accurate tumor resections.[55] Indocyanine green, approved by the Food and Drug Administration, has been explored for this application.[56] The significant advantage of NIR fluorescence, particularly its much lower tissue background noise, undoubtedly makes it a more ideal modality for guiding tumor resections during surgical therapy. Ni et al achieved precise surgical removal of abdominal metastatic tumors using the aforementioned NIR-emitting afterglow AIE dot (Fig. 7A).[28] Utilizing NIR-emitting afterglow AIE dots, it demonstrates effective passive tumor-targeting capability, illuminating nearly all tumor nodules, particularly submillimeter ones (Fig. 7B). Additionally, leveraging afterglow imaging enables minimal background interference. Subsequently, surgical therapy was performed to remove the tumors by surgeons who were unaware of the images and relied on their experience. A large number of tumors, most of which were >1 mm, were excised after unguided surgical therapy (Fig. 7C). This is because submillimeter tumors are in the early stages of cancer and are indeed difficult for surgeons to detect. In the second surgical therapy guided by afterglow imaging, the surgeon almost excised all tiny tumor nodules until there was no residual afterglow signal in the abdominal cavity. This demonstrates the excellent performance of NIR-emitting afterglow AIE dots in image-guided cancer surgical therapy. Wu et al reported a novel organic afterglow probe called $F1^{2+}$-ANP-Gal, which can be used for the localization of liver cancer during surgery.[31] In the study, $F1^{2+}$-ANP-Gal probe was used, and intense afterglow signals were generated through irradiation to accurately locate liver cancer tissue. This organic afterglow probe exhibits high sensitivity and noninvasiveness, allowing real-time imaging of liver cancer tissue and providing precise localization information for surgery. Additionally, the study demonstrated the ability of this organic afterglow probe to combine with tissue staining techniques, enabling precise delineation of the edges of liver cancer tissue. In conclusion, the organic afterglow probe $F1^{2+}$-ANP-Gal holds great potential as a valuable tool for guiding liver cancer surgery. Xie et al developed an amphiphilic poly(*p*-phenylenevinylene) derivatives that can self-assemble into the nanoagent (SPPVN) in biological solutions and emit near-infrared afterglow luminescence.[57] Compared to other reported near-infrared fluorescence imaging probes, SPPVN demonstrates superior sensitivity and is capable of detecting tumors with much smaller volumes. It can rapidly detect xenograft tumors as small as 1 mm^3 and even tiny peritoneal metastatic tumors that are almost invisible to the naked eye.

4.2 Photodynamic therapy

When irradiated by light, the photosensitizer can generate reactive oxygen species (ROS) that possess cytotoxicity and can kill cancer cells, thereby achieving therapeutic effects through a process known as photodynamic therapy (PDT).[58] Due to its highly spatial and temporal control over the therapy process, PDT has been employed in various cancer therapy.[59] However, the unknown ROS dosage during cancer therapy may induce the uncertainty of anticancer efficacy.[60] Liao et al constructed afterglow nanoreporters using the semiconducting polymer NIR-3, for precise and noninvasive early monitoring of the effectiveness of PDT (Fig. 8A).[39] As the NIR-3's afterglow luminescence is dependent on $^1O_2$, the afterglow intensity correlates closely with the tumor inhibition rates. Experimental results demonstrate

Table 1

Properties and therapy pathways of designed OALPs.

OALPs	Design strategy	λ_{em}*	Brightness†	Therapy pathways	Reference
AGL-AIE dots	Coencapsulation/near-infrared	650 nm	2.0×10^6	Surgical therapy	[28]
$F1^{2+}$-ANP-Gal	Coencapsulation/response/near-infrared	780 nm	3.0×10^5	Surgical therapy	[31]
SCAN	Coencapsulation/response	500 nm	3.0×10^7	Immunotherapy	[32]
RAN1	Coencapsulation/ratiometer	AF1 = 600 nm AF2 = 830 nm	4.0×10^5	Immunotherapy	[35]
Q-TPP-DO	Conjugation/near-infrared	670 nm	1.8×10^8	Surgical therapy	[36]
NIR-3	Conjugation/near-infrared	800–820 nm	1.2×10^6	Photodynamic therapy	[39]
MRAP-cRGD	Conjugation/response/near-infrared	770 nm	1.3×10^6	Radiodynamic therapy	[43]
MAS-pH	Conjugation/response/near-infrared	690–770 nm	1.0×10^6	Chemotherapy	[40]
SPN_{CT}	Coencapsulation	600 nm	1.4×10^5	Photothermal therapy	[50]
PA-AGL NPs	Coencapsulation/response	625 nm	1.2×10^9	Immunotherapy	[33]
PFODBT@CPPO	Coencapsulation/near-infrared	690–770 nm	1.0×10^7	Photodynamic therapy	[51]
TD-Grz-BHQ	Coencapsulation/response	630 nm	7.0×10^7	Immunotherapy	[52]
AIE/B-AGL-HCPT NPs	Coencapsulation/response/near-infrared	660 nm	2.0×10^6	Chemotherapy	[53]
APtN	Coencapsulation/response	550 nm	2.0×10^5	Chemotherapy	[54]

SBR refers to the tumor to the paratumoral tissue unless specified.

*λ_{em} is the highest afterglow emission wavelength.

†The unit of afterglow brightness is p s^{-1} cm^{-2} sr^{-1}.

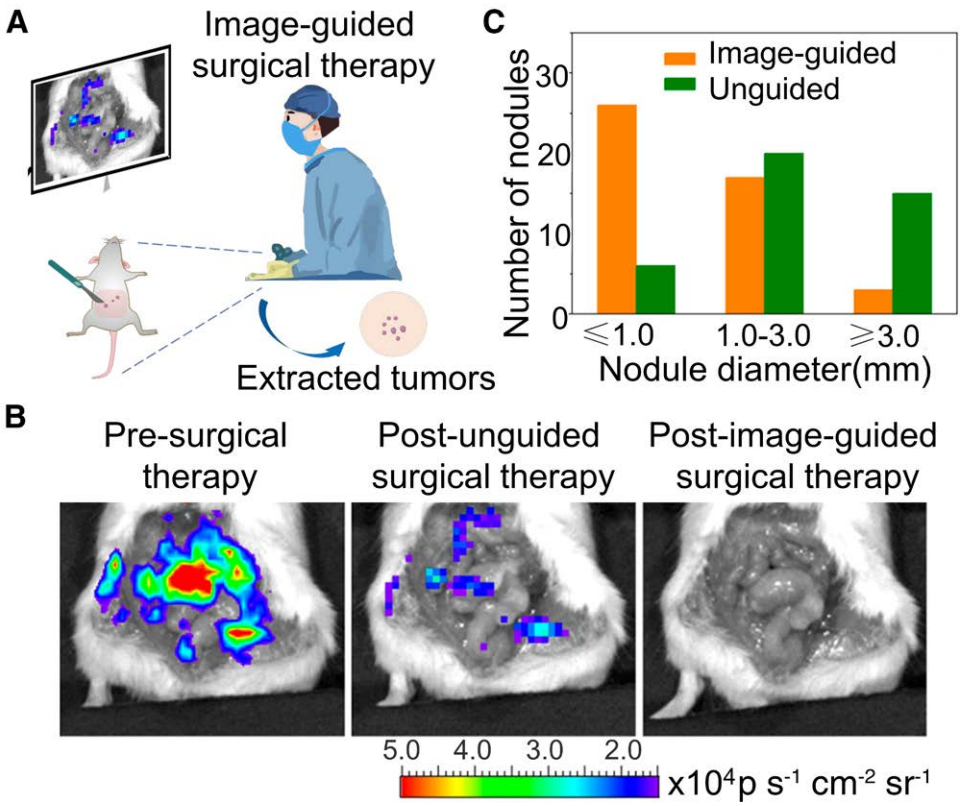

Figure 7. OALPs for surgical therapy. (A) Scheme illustrating image-guided surgical therapy. (B) Afterglow imaging of the opened peritoneal cavity at various stages of surgical therapy in tumor-bearing mice, following intravenous injection of NIR-emitting afterglow AIE dots. (C) The size distribution of tumor nodules resected from the mouse in (B) after the first unguided surgical therapy and the second afterglow image-guided surgical therapy. Adapted with permission from Ni et al.[28]

that with increasing injection dosage, mice exhibit enhanced afterglow luminescence in the tumor area (Fig. 8B). As the injection dosage of NIR-3 increases, the tumor inhibition rate also significantly increases and the afterglow intensity in the tumor region correlates with the tumor inhibition rate (Fig. 8C). The afterglow luminescence can be utilized as an early-stage therapy metric prior to tumor volume reduction, measuring the efficacy of $^1O_2$-mediated anticancer activity. Wang et al developed a cyclic amplification of the afterglow luminescent nanoreporter called PFODBT@CPPO, which can be used to real-time visualize light-induced ROS and monitor ROS-mediated cancer treatment efficacy.[51] The afterglow intensity of the nanoreporter can also be utilized to adjust treatment parameters such as dosage and irradiation time, enabling personalized treatment plans and avoiding ineffective or excessive medical interventions.

4.3 Photothermal therapy

Photothermal therapy (PTT) effectively utilizes photothermal agents to convert light energy into heat, thereby killing cancer cells.[61] Zhen et al coencapsulated OALPs and photothermal agents to prepare nanococktail. Following intravenous administration, nanococktail passively targets and accumulates in tumors (Fig. 9A).[50] Subsequently, nanococktail can absorb light, converting light energy into heat to achieve PTT. During PTT, as the decomposition of 1,2-dioxetane is temperature-dependent, the afterglow intensity of nanococktail also exhibits temperature dependence, enabling monitoring of PTT via afterglow imaging (Fig. 9B). Furthermore, due to the high tissue penetration and imaging sensitivity of afterglow luminescence, it holds potential for monitoring deep-tissue temperatures.

4.4 Radiodynamic therapy

Compared to light, X-rays have greater tissue penetration capability, making them more suitable for deep-tissue diagnostic imaging and cancer therapy.[62] Inspired by PDT, X-rays can be utilized as an energy source to achieve radiodynamic therapy (RDT).[63] Due to the localized production of cytotoxic ROS by the therapeutic agent, RDT can minimize radiation damage to normal tissues. Huang et al utilized the previously mentioned MRAP and modified it with the tumor-targeting moiety cRGD to obtain MRAP-cRGD, which was successfully employed in brain tumor radiodynamic theranostics.[43] MRAP has both tumor-activatable afterglow luminescence and the ability to produce $^1O_2$ (Fig. 10A). Under low-dose X-ray irradiation of 5 mGy, radioafterglow imaging (RAI) was performed, showing that the radioafterglow in orthotopic glioblastoma gradually increased, reaching its peak at 24 hours, with significantly higher afterglow intensity compared to other groups (Fig. 10B, C). Subsequently, tumor growth was continuously monitored via bioluminescence signal. The results revealed that following high-dose 0.8 Gy RDT, tumor growth was completely inhibited in the MRAP group, whereas other groups did not exhibit significant tumor regression or inhibition (Fig. 10D).

4.5 Chemotherapy

Chemotherapy is a method of cancer therapy by using specific drugs to kill or control the growth of cancer cells, thereby helping patients alleviate symptoms, control the disease, and extend survival.[64] However, chemotherapy drugs not only affect tumors but may also impact normal tissues. In order to

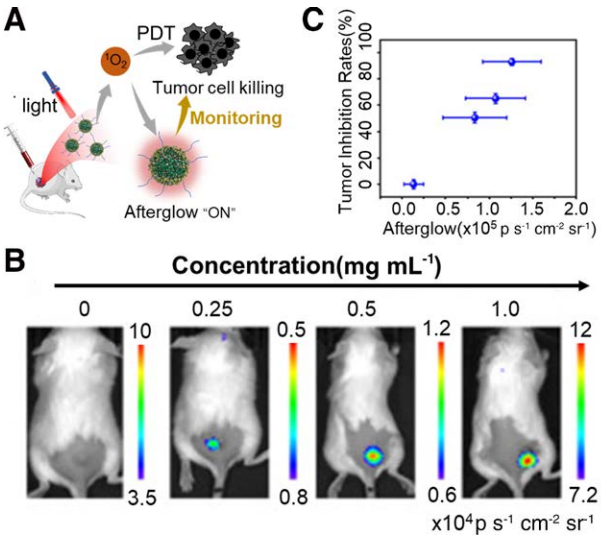

Figure 8. OALPs for photodynamic therapy. (A) Scheme illustrating afterglow imaging monitoring photodynamic therapy. (B) Afterglow images of mice with subcutaneous tumors injected intratumorally with different concentrations of NIR-3. (C) Quantification of in vivo afterglow intensities of tumor as a function of tumor growth inhibition rates. Adapted with permission from Liao et al.[39]

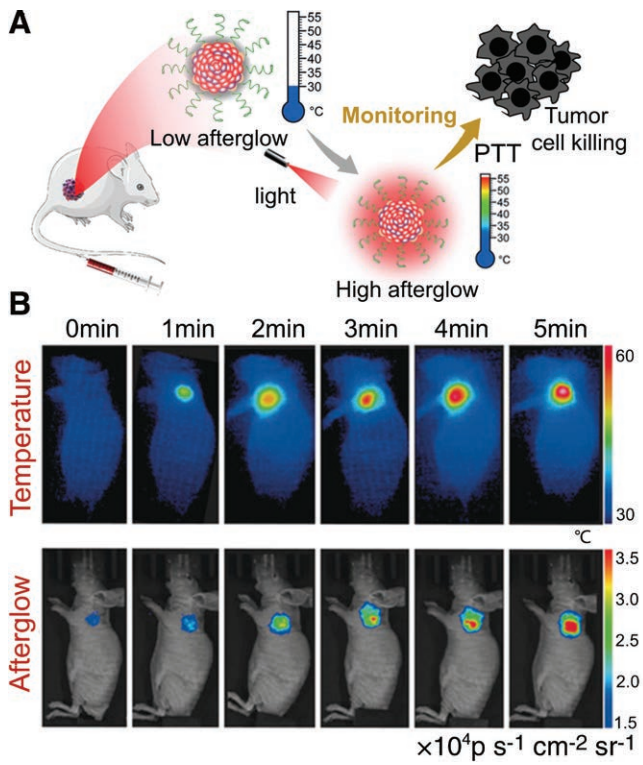

Figure 9. OALPs for photothermal therapy. (A) Scheme illustrating afterglow imaging monitoring photothermal therapy. (B) Thermal and afterglow imaging of mice with subcutaneous tumors after intravenous injection of nanococktail, undergoing light irradiation for various durations. Adapted with permission from Zhen et al.[50]

mitigate damage to normal tissues, a series of prodrugs have been developed for cancer therapy, which are inactive until they reach the tumor microenvironment.[65] Upon response to biomarkers in the tumor microenvironment, they release active drugs, thus partially avoiding toxicity to normal tissues. He et al developed an afterglow protheranostic nanoassembly by coencapsulating an afterglow prodrug and an afterglow initiator.[54] The afterglow prodrug is comprised of the chemotherapy drug 5'-deoxy-5-fluorouridine (5DFUR) linked to an afterglow substrate via a boronic ester bond responsive to H_2O_2. Once the nanoassembly reaches the tumor microenvironment, it reacts with overexpressed H_2O_2, releasing 5DFUR and simultaneously activates afterglow luminescence (Fig. 11A). Hence, there is a good linear correlation (R^2 = 0.9857) between the afterglow luminescence intensity and the release of chemotherapy drugs (Fig. 11B), enabling real-time tracking of drug activation and release in vivo, which holds promise for guiding physicians in formulating drug regimens. Gao et al also reported an activatable NIR afterglow protheranostic nanoassembly by coencapsulating afterglow prodrugs and NIR emissive AIE luminogens.[53] The afterglow prodrug consists of chemotherapy drug hydroxycamptothecin (HCPT) and an afterglow substrate linked through the carbonate group, which is caged by an $ONOO^-$-responsive phenylborate group. The AIE luminogens serve as both the afterglow initiator and afterglow relay unit. The activatable NIR afterglow luminescence serves as the signal readout to monitor and quantify drug release status and theranostic response. Lei et al developed a pH-responsive afterglow probe called MAS-pH, which can be used to monitor the effects of the oxidative phosphorylation inhibitor tamoxifen on tumor glycolysis and chemotherapy outcomes in living mice.[40] The experimental results demonstrate that increasing the dose of tamoxifen leads to an increase in the afterglow signal, a decrease in tumor pH, an elevation in glycolytic levels, and an enhancement in chemotherapy outcomes. Therefore, MAS-pH shows great potential in evaluating tumor glycolysis, monitoring chemotherapy resistance, and screening effective approaches to regulate glycolysis.

4.6 Immunotherapy

While immunotherapy holds great promise in cancer therapy, patient responses vary widely across different types of cancer, resulting in significant individual differences.[66] Due to the proven correlation between response rates and therapy outcomes with the proinflammatory tumor microenvironment, there is a critical need for cancer immunotherapeutic agents capable of providing real-time feedback on the proinflammatory tumor microenvironment to guide immunotherapy.[67] Xu et al coencapsulated a M1-like macrophages (M1)-polarizing prodrug caged with a $^1O_2$-cleavable moiety in the responsive sonoafterglow nanoparticles, creating a sonoafterglow cancer nanoimmunotheranostic probe (SCAN).[32] The sonodynamic effect (generation of $^1O_2$) and sonoafterglow are activated only in the proinflammatory tumor microenvironment when high levels of $ONOO^-$ are present (Fig. 12A). The generated $^1O_2$ by SCAN triggers the cleavage of the M1-polarizing prodrug, thereby activating immunotherapy in situ. Researchers defined the difference in sonoafterglow intensity between sequential doses as ΔS and investigated its relationship with the proinflammatory state levels of tumor M1 characteristics (Fig. 12B, C). Under the same ultrasound irradiation, SCAN induced a significantly higher number of M1 macrophages compared to the SCANc group (lacking the M1-polarizing prodrug) after the fourth dose (Fig. 12D). The increasing trend of M1 macrophage population was consistent with the sonoafterglow in each group. Tumor suppression experiments revealed that single sonodynamic therapy mediated by SCAN-C failed to eradicate the tumor, whereas the combination of immunotherapy with SCAN resulted in complete tumor eradication (Fig. 12E). These results confirm the efficacy of SCAN-mediated

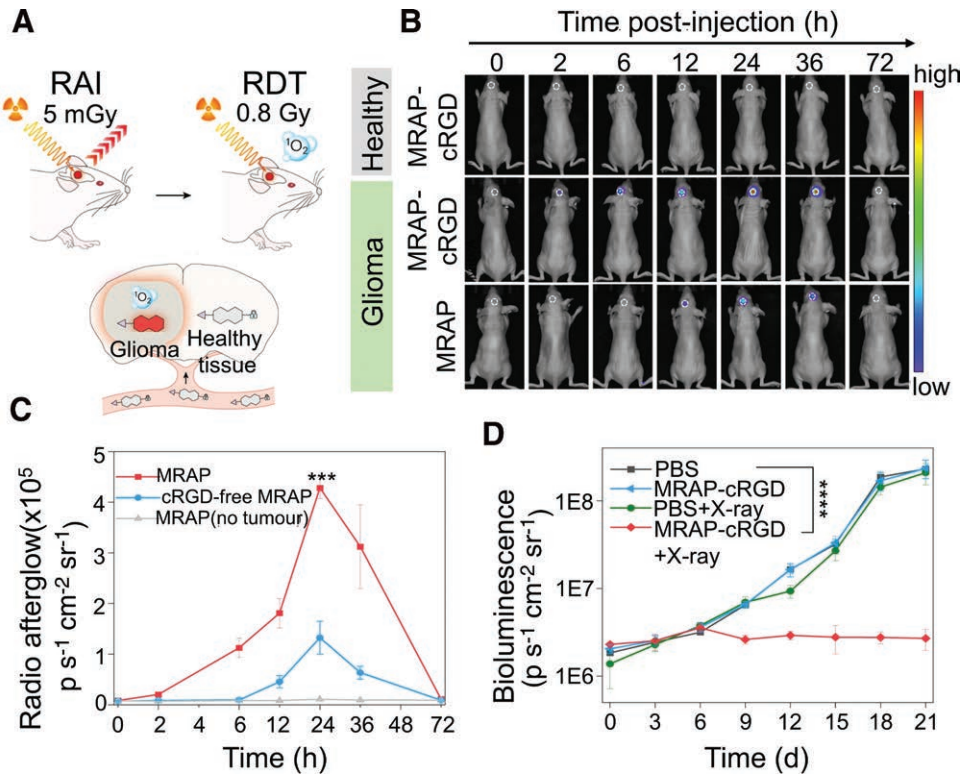

Figure 10. OALPs for radiodynamic therapy. (A) Scheme illustrating RAI monitoring RDT. (B) Radioafterglow images of orthotopic glioblastoma (glioma) and healthy mice at different time points after an intravenous injection of MRAP-cRGD and MRAP. (C) The quantitative analysis of radioafterglow intensities in the mouse brain region is presented in (B). (D) Tumor growth of orthotopic glioblastoma mice after the indicated therapies. Adapted with permission from Huang et al.[43]

immunotherapy. Chen et al developed a novel organic afterglow probe called PA-AGL NPs, which can be used for fast screening of antitumor drugs capable of inducing immunogenic cell death (ICD).[33] Specifically, preirradiated PA-AGL nanoparticles can visualize the infiltration process of neutrophils by measuring the activated afterglow intensity of $ONOO^-$. The activation of ICD requires the activation of inflammation-related immune cells, particularly neutrophils. $ONOO^-$, as a ROS associated with inflammation, can be generated during the inflammatory process. Therefore, ICD drugs may promote the immunogenic conversion of tumors by activating the inflammatory response and immune cells. Liu et al developed an ultrasound-induced afterglow luminescent probes called RAN1, which enables reliable quantification of nitric oxide (NO) and can be used for afterglow imaging in macrophage-modulated immunotherapy.[35] The researchers first treated RAW264.7 macrophages with different macrophage polarization modulators and then performed afterglow imaging by administering RAN1 to these cells. It was observed that the afterglow intensity was correlated with the degree of macrophage polarization. Furthermore, the researchers observed a strong correlation between afterglow intensity, macrophage polarization, and the anticancer effect in 4T1 tumor-bearing mice. In conclusion, ratiometric afterglow imaging can serve as an effective method for evaluating macrophage polarization and screening modulators, enabling real-time monitoring of macrophage-modulated immunotherapy. The same research group has developed an ultrasound-induced afterglow luminescence nanoprobe called TD-Grz-BHQ, which can be used to monitor the granzyme B levels and the immune response in living mice.[52] The afterglow intensity of TD-Grz-BHQ was detected in CT-26 tumors following anti-PDL1 treatment and exhibited a higher level compared to the signal observed in 4T1 tumors. The higher afterglow intensity of TD-Grz-BHQ in CT-26 tumors following anti-PDL1 treatment can be attributed to the elevated levels of granzyme B, $CD8^+$ T cells, and NK cells. In conclusion, ultrasound-induced afterglow luminescence nanoprobe can be used to monitor the immune response and evaluate the efficacy of immunotherapy.

5. The biosafety and metabolic pathways

Currently, OALPs used in cancer theranostics often need to be formulated into nanoparticles that integrate different components to function collectively and enhance tumor targeting and bioavailability. Therefore, the biocompatibility and metabolic pathways of these carriers are critical considerations. Organic nanoparticles are typically composed of natural or synthetic materials with high biocompatibility, such as proteins, polysaccharides, and lipids, making them more readily accepted by biological systems in vivo.[52] Moreover, to enhance the safety of carriers, their surfaces are commonly modified with polyethylene glycol, which effectively reduces protein adsorption in vivo, decreases immune system recognition and clearance, and reduces immunogenicity while prolonging circulation time in the bloodstream.[68] Additionally, organic nanoparticles can be tailored to target specific tissues or cells by adjusting their surface chemistry or attaching targeting molecules. This targeting helps to increase the local concentration of the drug, reducing adverse effects on healthy tissues. Regarding metabolic pathways, unlike small molecule probes or drugs, which are easily excreted through urine or metabolized by the liver, nanoparticles, due to the EPR effect, tend to accumulate at tumor sites.[69]

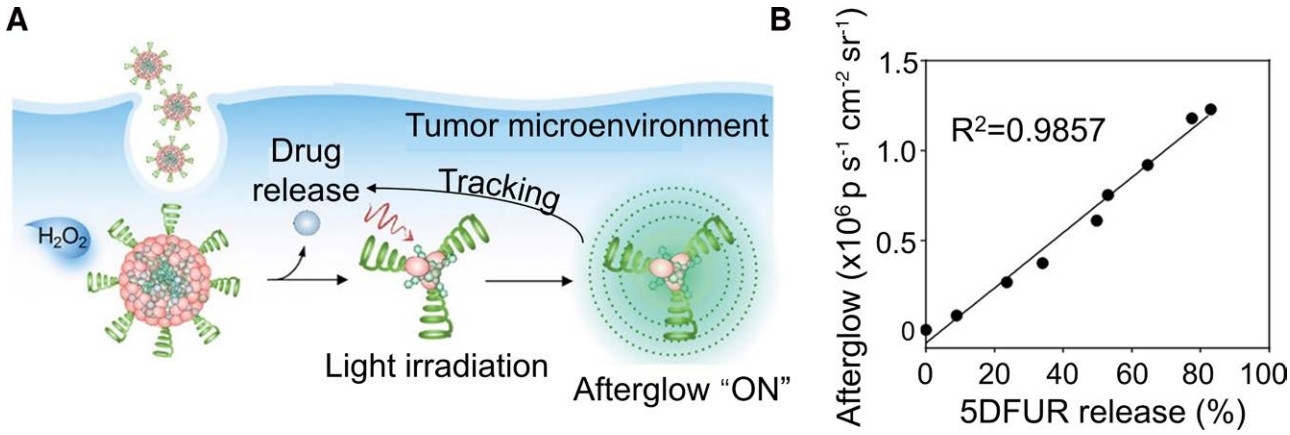

Figure 11. OALPs for chemotherapy. (A) Scheme illustrating afterglow luminescence tracking drug release status. (B) Correlation between afterglow intensities and the percentage of 5DFUR release. Adapted with permission from He et al.[54]

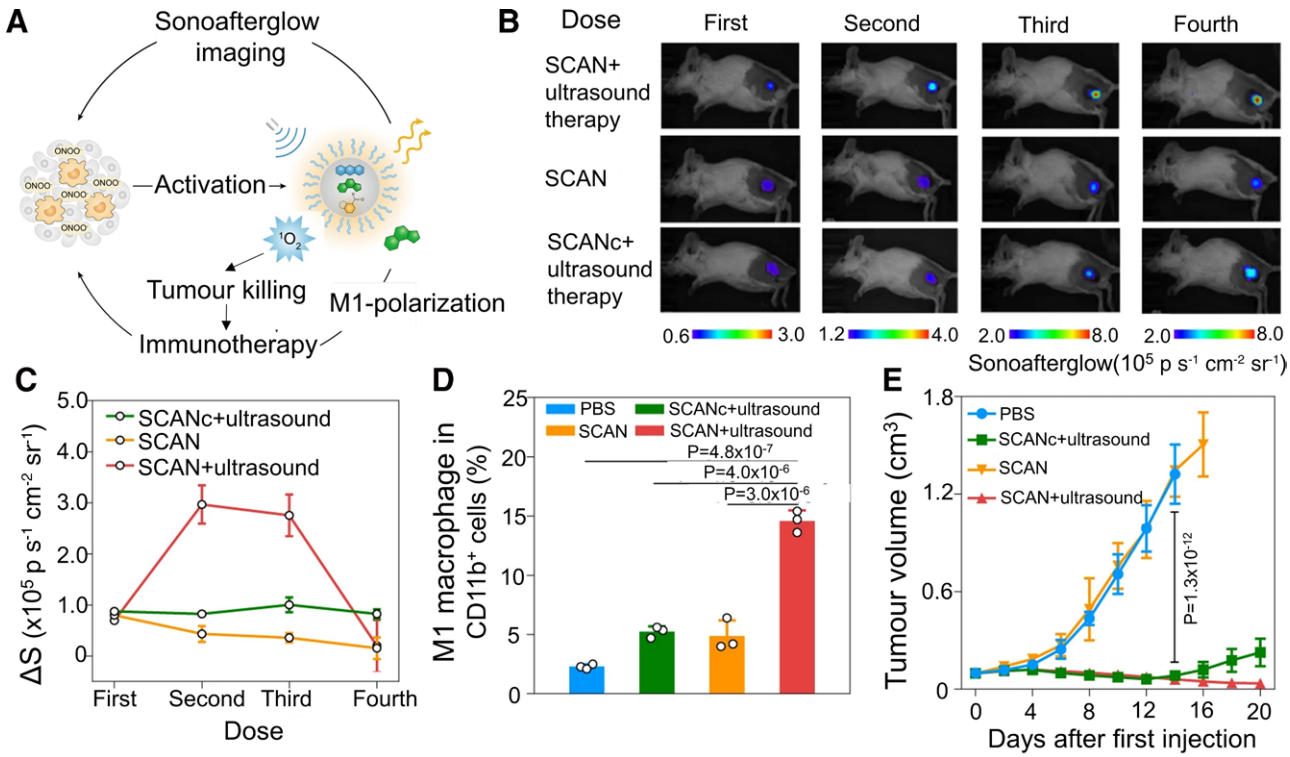

Figure 12. OALPs for immunotherapy. (A) Scheme illustrating sonoafterglow-guided immunotherapy. (B) Sonoafterglow images of tumor-bearing mice administered in increasing doses after the indicated therapies. (C) Quantification of the difference in afterglow intensity (ΔS) between sequential doses is presented in (B). (D) Quantification of intratumoral M1 macrophages using flow cytometry. (E) Tumor growth of mice after the indicated therapies. Adapted with permission from Xu et al.[32]

However, larger nanoparticles are likely to remain in the reticuloendothelial system (such as the liver and spleen), which may lead to long-term biological accumulation and potential toxicity issues. Therefore, to enhance the metabolism and safety of nanoparticles, it is advisable to develop smaller and more uniformly distributed nanoparticles, as their reduced size facilitates renal excretion.[70]

6. Conclusions and outlook

Despite significant progress, there are considerable challenges that need to be addressed before clinical translation. We identify the following challenges in this field. (1) While X-ray and ultrasound-excited afterglows have resolved the issue of penetration depth, there is still a lack of OALPs emitting in the NIR-II window (1000–1700 nm), which can reduce light scattering in tissues. (2) In tumor hypoxic microenvironments, the efficiency of high oxygen-dependent type I photosensitizers in producing $^1O_2$ is not optimal. Therefore, there is a need to develop OALPs mediated by other ROS, such as those based on type II photosensitizers with lower oxygen consumption. (3) Current afterglow imaging studies mainly focus on cancer research, neglecting other life-threatening or chronic diseases such as coronary heart disease, diabetes, neurological disorders, and autoimmune diseases. (4) There are few reports on ratiometric afterglow. More research efforts should be directed toward improving the quality and reliability of afterglow imaging using this strategy or developing new techniques such as afterglow lifetime imaging

to further enhance imaging quality. In conclusion, OALPs offer significant advantages in disease diagnosis and therapy. We hope this review will inspire researchers interested in developing OALPs to collectively advance their application in the biomedical field.

Acknowledgments

This work was supported by the National Natural Science Foundation of China (52225310) and Tianjin Key Medical Discipline (Specialty) Construction Project.

Conflicts of interests

The authors declare that they have no conflicts of interest.

References

[1] Kenry, Duan Y, Liu B. Recent advances of optical imaging in the second near-infrared window. *Adv Mater*. 2018;30(47):1802394.
[2] Li J, Pu K. Development of organic semiconducting materials for deep-tissue optical imaging, phototherapy and photoactivation. *Chem Soc Rev*. 2019;48(1):38–71.
[3] Cheng P, Pu K. Molecular imaging and disease theranostics with renal-clearable optical agents. *Nat Rev Mater*. 2021;6(12):1095–1113.
[4] Culley S, Albrecht D, Jacobs C, et al. Quantitative mapping and minimization of super-resolution optical imaging artifacts. *Nat Methods*. 2018;15(4):263–266.
[5] Cosco ED, Spearman AL, Ramakrishnan S, et al. Shortwave infrared polymethine fluorophores matched to excitation lasers enable non-invasive, multicolour in vivo imaging in real time. *Nat Chem*. 2020;12(12):1123–1130.
[6] Yoon S, Kim M, Jang M, et al. Deep optical imaging within complex scattering media. *Nat Rev Phys*. 2020;2(3):141–158.
[7] Jiang Y, Pu K. Molecular probes for autofluorescence-free optical imaging. *Chem Rev*. 2021;121(21):13086–13131.
[8] Yeh H-W, Ai H-W. Development and applications of bioluminescent and chemiluminescent reporters and biosensors. *Annu Rev Anal Chem (Palo Alto Calif)*. 2019;12:129–150.
[9] Vacher M, Fdez Galván I, Ding B-W, et al. Chemi-and bioluminescence of cyclic peroxides. *Chem Rev*. 2018;118(15):6927–6974.
[10] Yang M, Huang J, Fan J, et al. Chemiluminescence for bioimaging and therapeutics: recent advances and challenges. *Chem Soc Rev*. 2020;49(19):6800–6815.
[11] Yan Y, Shi P, Song W, et al. Chemiluminescence and bioluminescence imaging for biosensing and therapy: in vitro and in vivo perspectives. *Theranostics*. 2019;9(14):4047–4065.
[12] Syed AJ, Anderson JC. Applications of bioluminescence in biotechnology and beyond. *Chem Soc Rev*. 2021;50(9):5668–5705.
[13] Shen H, Liao S, Li Z, et al. Organic afterglow nanoparticles in bioapplications. *Chemistry*. 2023;29(42):e202301209.
[14] Wang X, Pu K. Molecular substrates for the construction of afterglow imaging probes in disease diagnosis and treatment. *Chem Soc Rev*. 2023;52(14):4549–4566.
[15] Yang X, Waterhouse GI, Lu S, et al. Recent advances in the design of afterglow materials: mechanisms, structural regulation strategies and applications. *Chem Soc Rev*. 2023;52:8005–8058.
[16] Wu Z, Midgley AC, Kong D, et al. Organic persistent luminescence imaging for biomedical applications. *Mater Today Bio*. 2022;17:100481.
[17] Yang L, Gai S, Ding H, et al. Recent progress in inorganic afterglow materials: mechanisms, persistent luminescent properties, modulating methods, and bioimaging applications. *Adv Opt Mater*. 2023;11(11):2202382.
[18] Xu M, Liu J, Su X, et al. Lanthanide-containing persistent luminescence materials with superbright red afterglow and excellent solution processability. *Sci China Chem*. 2021;64:2125–2133.
[19] Li J, Chang X, Chen X, et al. Toxicity of inorganic nanomaterials in biomedical imaging. *Biotechnol Adv*. 2014;32(4):727–743.
[20] Wang X, Zhong X, Li J, et al. Inorganic nanomaterials with rapid clearance for biomedical applications. *Chem Soc Rev*. 2021;50(15):8669–8742.
[21] Yang M, Zeng Z, Lam JW, et al. State-of-the-art self-luminescence: a win–win situation. *Chem Soc Rev*. 2022;51:8815–8831.
[22] Gao M, Yu F, Lv C, et al. Fluorescent chemical probes for accurate tumor diagnosis and targeting therapy. *Chem Soc Rev*. 2017;46(8):2237–2271.
[23] Jeyamogan S, Khan NA, Siddiqui R. Application and importance of theranostics in the diagnosis and treatment of cancer. *Arch Med Res*. 2021;52(2):131–142.
[24] Ko C-N, Li G, Leung C-H, et al. Dual function luminescent transition metal complexes for cancer theranostics: the combination of diagnosis and therapy. *Coord Chem Rev*. 2019;381:79–103.
[25] Hong G, Antaris AL, Dai H. Near-infrared fluorophores for biomedical imaging. *Nat Biomed Eng*. 2017;1(1):0010.
[26] Li C, Chen G, Zhang Y, et al. Advanced fluorescence imaging technology in the near-infrared-II window for biomedical applications. *J Am Chem Soc*. 2020;142(35):14789–14804.
[27] Jiang Y, Huang J, Zhen X, et al. A generic approach towards afterglow luminescent nanoparticles for ultrasensitive in vivo imaging. *Nat Commun*. 2019;10(1):2064.
[28] Ni X, Zhang X, Duan X, et al. Near-infrared afterglow luminescent aggregation-induced emission dots with ultrahigh tumor-to-liver signal ratio for promoted image-guided cancer surgery. *Nano Lett*. 2018;19(1):318–330.
[29] Zeng Y, Dou T, Ma L, et al. Biomedical photoacoustic imaging for molecular detection and disease diagnosis: "Always-On" and "Turn-On" probes. *Adv Sci*. 2022;9(25):e2202384.
[30] Li X, Yin C, Liew SS, et al. Organic semiconducting luminophores for near-infrared afterglow, chemiluminescence, and bioluminescence imaging. *Adv Funct Mater*. 2021;31(46):2106154.
[31] Wu L, Ishigaki Y, Hu Y, et al. H2S-activatable near-infrared afterglow luminescent probes for sensitive molecular imaging in vivo. *Nat Commun*. 2020;11(1):446.
[32] Xu C, Huang J, Jiang Y, et al. Nanoparticles with ultrasound-induced afterglow luminescence for tumour-specific theranostics. *Nat Biomed Eng*. 2023;7(3):298–312.
[33] Chen C, Gao H, Ou H, et al. Amplification of activated near-infrared afterglow luminescence by introducing twisted molecular geometry for understanding neutrophil-involved diseases. *J Am Chem Soc*. 2022;144(8):3429–3441.
[34] Duan X, Zhang GQ, Ji S, et al. Activatable persistent luminescence from porphyrin derivatives and supramolecular probes with imaging-modality transformable characteristics for improved biological applications. *Angew Chem Int Ed*. 2022;61(24):e202116174.
[35] Liu Y, Teng L, Lyu Y, et al. Ratiometric afterglow luminescent nanoplatform enables reliable quantification and molecular imaging. *Nat Commun*. 2022;13(1):2216.
[36] Yang L, Zhao M, Chen W, et al. A highly bright near-infrared afterglow luminophore for activatable ultrasensitive in vivo imaging. *Angew Chem*. 2024;136(4):e202313117.
[37] Miao Q, Xie C, Zhen X, et al. Molecular afterglow imaging with bright, biodegradable polymer nanoparticles. *Nat Biotechnol*. 2017;35(11):1102–1110.
[38] Cui D, Xie C, Li J, et al. Semiconducting photosensitizer-incorporated copolymers as near-infrared afterglow nanoagents for tumor imaging. *Adv Healthcare Mater*. 2018;7(18):1800329.
[39] Liao S, Wang Y, Li Z, et al. A novel afterglow nanoreporter for monitoring cancer therapy. *Theranostics*. 2022;12(16):6883–6897.
[40] Lei L, Yang F, Meng X, et al. Noninvasive imaging of tumor glycolysis and chemotherapeutic resistance via de novo design of molecular afterglow scaffold. *J Am Chem Soc*. 2023;145(44):24386–24400.
[41] Liu Y, Teng L, Lou X-F, et al. "Four-In-One" design of a hemicyanine-based modular scaffold for high-contrast activatable molecular afterglow imaging. *J Am Chem Soc*. 2023;145(9):5134–5144.
[42] Hong Z, Chen Z, Chen Q, et al. Advancing X-ray luminescence for imaging, biosensing, and theragnostics. *Acc Chem Res*. 2022;56(1):37–51.
[43] Huang J, Su L, Xu C, et al. Molecular radio afterglow probes for cancer radiodynamic theranostics. *Nat Mater*. 2023;22(11):1421–1429.
[44] Siegel RL, Miller KD, Wagle NS, et al. Cancer statistics, 2023. *CA Cancer J Clin*. 2023;73(1):17–48.
[45] Rosenblum D, Joshi N, Tao W, et al. Progress and challenges towards targeted delivery of cancer therapeutics. *Nat Commun*. 2018;9(1):1410.
[46] Attia MF, Anton N, Wallyn J, et al. An overview of active and passive targeting strategies to improve the nanocarriers efficiency to tumour sites. *J Pharm Pharmacol*. 2019;71(8):1185–1198.

[47] Hui Y, Wibowo D, Liu Y, et al. Understanding the effects of nanocapsular mechanical property on passive and active tumor targeting. *ACS Nano*. 2018;12(3):2846–2857.
[48] Zhang J, Ning L, Huang J, et al. Activatable molecular agents for cancer theranostics. *Chem Sci*. 2020;11(3):618–630.
[49] Li J, Zhang Y, Qu J, et al. Phototheranostic nanoagents for imaging-guided treatment of oral cancer. *Chin J Chem*. 2023;41(13):1624–1636.
[50] Zhen X, Xie C, Pu K. Temperature-correlated afterglow of a semiconducting polymer nanococktail for imaging-guided photothermal therapy. *Angew Chem*. 2018;130(15):4002–4006.
[51] Wang Y, Song G, Liao S, et al. Cyclic amplification of the afterglow luminescent nanoreporter enables the prediction of anti-cancer efficiency. *Angew Chem Int Ed Engl*. 2021;60(36):19779–19789.
[52] Wang Y, Yi Z, Guo J, et al. In vivo ultrasound-induced luminescence molecular imaging. *Nat Photon*. 2024;18:334–343.
[53] Gao Z, Jia S, Ou H, et al. An activatable near-infrared afterglow theranostic prodrug with self-sustainable magnification effect of immunogenic cell death. *Angew Chem Int Ed*. 2022;61(40):e202209793.
[54] He S, Xie C, Jiang Y, et al. An organic afterglow protheranostic nanoassembly. *Adv Mater*. 2019;31(32):1902672.
[55] Li J, Zhang GQ, Zhang Y, et al. Building highly light-harvesting near-infrared AIEgens using triazole-based luminescent core for improved intravital afterglow imaging. *Adv Funct Mater*. 2023;33(19):2212380.
[56] Egloff-Juras C, Bezdetnaya L, Dolivet G, et al. NIR fluorescence-guided tumor surgery: new strategies for the use of indocyanine green. *Int J Nanomed*. 2019;14:7823–7838.
[57] Xie C, Zhen X, Miao Q, et al. Self-assembled semiconducting polymer nanoparticles for ultrasensitive near-infrared afterglow imaging of metastatic tumors. *Adv Mater*. 2018;30(21):1801331.
[58] Gunaydin G, Gedik ME, Ayan S. Photodynamic therapy—current limitations and novel approaches. *Front Chem*. 2021;9:691697.
[59] Lan M, Zhao S, Liu W, et al. Photosensitizers for photodynamic therapy. *Adv Healthcare Mater*. 2019;8(13):1900132.
[60] Zhou L, Zhang P, Wang H, et al. Smart nanosized drug delivery systems inducing immunogenic cell death for combination with cancer immunotherapy. *Acc Chem Res*. 2020;53(9):1761–1772.
[61] Zhi D, Yang T, O'hagan J, et al. Photothermal therapy. *J Control Release*. 2020;325:52–71.
[62] Larue L, Mihoub AB, Youssef Z, et al. Using X-rays in photodynamic therapy: an overview. *Photochem Photobiol Sci*. 2018;17(11):1612–1650.
[63] Liu J, Hu F, Wu M, et al. Bioorthogonal coordination polymer nanoparticles with aggregation-induced emission for deep tumor-penetrating radio-and radiodynamic therapy. *Adv Mater*. 2021;33(9):2007888.
[64] Bukowski K, Kciuk M, Kontek R. Mechanisms of multidrug resistance in cancer chemotherapy. *Int J Mol Sci*. 2020;21(9):3233.
[65] Liu L, Liu F, Liu D, et al. A smart theranostic prodrug system activated by reactive oxygen species for regional chemotherapy of metastatic cancer. *Angew Chem*. 2022;134(12):e202116807.
[66] Conforti F, Pala L, Bagnardi V, et al. Cancer immunotherapy efficacy and patients' sex: a systematic review and meta-analysis. *Lancet Oncol*. 2018;19(6):737–746.
[67] Sadeghi Rad H, Monkman J, Warkiani ME, et al. Understanding the tumor microenvironment for effective immunotherapy. *Med Res Rev*. 2021;41(3):1474–1498.
[68] Shi L, Zhang J, Zhao M, et al. Effects of polyethylene glycol on the surface of nanoparticles for targeted drug delivery. *Nanoscale*. 2021;13(24):10748–10764.
[69] Llop J, Lammers T. Nanoparticles for cancer diagnosis, radionuclide therapy and theranostics. *ACS Nano*. 2021;15(11):16974–16981.
[70] Du B, Yu M, Zheng J. Transport and interactions of nanoparticles in the kidneys. *Nat Rev Mater*. 2018;3(10):358–374.

How to cite this article: Gao Z, Zhang Y, Liu Q, Ding D. Mechanism and design of organic afterglow luminescent probes for cancer theranostics. MedMat 2024;1(1):e00003. doi: 10.1097/mm9.0000000000000003